

Molecular origin of driving-dependent friction in fluids

Matthias Post, Steffen Wolf, and Gerhard Stock

Biomolecular Dynamics, Institute of Physics, Albert Ludwigs University, 79104 Freiburg, Germany

(Dated: April 8, 2022)

The friction coefficient of fluids may become a function of the velocity at increased external driving. This non-Newtonian behavior is of general theoretical interest as well as of great practical importance, e.g., for the design of lubricants. While the effect has been observed in large-scale atomistic simulations of bulk liquids, its theoretical formulation and microscopic origin is not well understood. Here we use dissipation-corrected targeted molecular dynamics, which pulls apart two tagged liquid molecules in the presence of surrounding molecules and analyzes this nonequilibrium process via a generalized Langevin equation. The approach is based on a second-order cumulant expansion of Jarzynski's identity, which is shown to be valid for fluids and therefore allows for an exact computation of the friction profile as well of the underlying memory kernel. We show that velocity-dependent friction in fluids results from an intricate interplay of near-order structural effects and the non-Markovian behavior of the friction memory kernel. For complex fluids such as the model lubricant $C_{40}H_{82}$, the memory kernel exhibits a stretched-exponential long-time decay, which reflects the multitude of timescales of the system.

I. INTRODUCTION

An object driven through a liquid at low to moderate velocities v encounters a drag force $f_{\text{fric}} = -v\Gamma$ with the Stokes' friction factor Γ . While Γ is a constant close to equilibrium, it may become a function of the velocity at increased driving. This so-called non-Newtonian behavior of liquids represents an intriguing topic of fundamental research in rheology and microrheology [1–3]. Applied to the shearing of a bulk liquid, the behavior is characterized either as “shear thickening”, i.e., an increase of internal friction and thus viscosity upon shearing, or “shear thinning” corresponding to a decrease of the friction [4]. The latter is of great practical importance, e.g., for the design of lubricants which aim to minimize friction and wear [5]. Non-Newtonian behavior is believed to result from structural changes within the liquid, such as the alignment of polymers along the shearing direction [6–9] or from the formation of molecule clusters [10–12].

As an alternative to microscopic studies that are based on large-scale molecular dynamics (MD) simulations, it is instructive to adopt a coarse-grained description that focuses on the friction experienced by a driven test molecule. Integrating out all degrees of freedom of the surrounding molecules, such theoretical formulations yield the friction in terms of time-dependent molecular correlation functions [13–19]. In contrast to sliding friction on surfaces whose driving dependence has been successfully studied using the Prandtl-Tomlinson model [20], the connection between the coarse-grained theoretical representation and the microscopic origin of velocity-dependent friction in condensed matter systems is only poorly understood.

In this work we want to amend this understanding by studying driving-dependent Stokes friction within the theoretical framework of dissipation-corrected targeted molecular dynamics (dcTMD) [21]. The method employs a constraint force f that effects a moving distance constraint $x = x_0 + vt$ with a constant velocity v [22], which

pulls apart two tagged molecules (the “system”) in the presence of the surrounding molecules (the “bath”) causing the friction (Fig. 1). In this way, dcTMD simulations resemble an active microrheology experiment, where an external force is applied to a tracer molecule [3]. The approach is based on Jarzynski's identity [23–25]

$$\Delta G = -\beta^{-1} \ln \langle e^{-\beta W} \rangle, \quad (1)$$

which estimates the free energy difference ΔG between two states of a system from the amount of work W done on this system to enforce the nonequilibrium process. Here the brackets denote an ensemble average over statistically independent nonequilibrium simulations starting from a common equilibrium state, and $\beta^{-1} = k_B T$ is the inverse temperature. To avoid problems associated with the poor convergence behavior of the exponential average (see below), often the second-order cumulant expansion of Jarzynski's identity is considered,

$$\Delta G = \langle W \rangle - \langle W_{\text{diss}} \rangle \approx \langle W \rangle - \frac{\beta}{2} \langle \delta W^2 \rangle, \quad (2)$$

where the first term represents the averaged external work performed on the system, and the second term corresponds to the mean dissipated work $\langle W_{\text{diss}}(x) \rangle$ of the process with $\delta W = W - \langle W \rangle$. Pulling the system from x_0 to x , we obtain [21]

$$\langle W(x) \rangle = \int_{x_0}^x dx' \langle f(x') \rangle, \quad (3)$$

$$\langle W_{\text{diss}} \rangle(x) = \frac{\beta}{2} \int_{x_0}^x dx' \int_{x_0}^x dx'' \langle \delta f(x') \delta f(x'') \rangle \quad (4)$$

$$= v \int_{x_0}^x dx' \Gamma(x'), \quad (5)$$

which relates the the dissipated work to the autocorrelation function of the constraint force $\delta f = f - \langle f \rangle$, and also provides a means to calculate the position-dependent

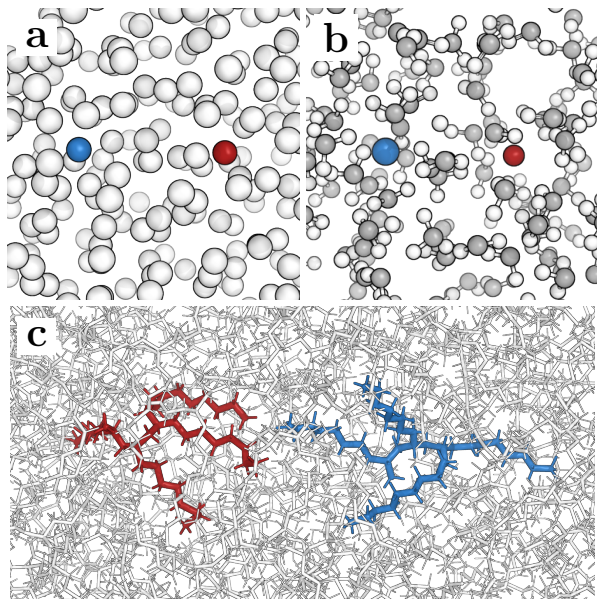


FIG. 1. To study the friction in fluids, two tagged molecules (in blue and red) are pulled apart using dissipation-corrected targeted molecular dynamics (dcTMD) [21]. Model systems considered include (a) a Lennard-Jones liquid, (b) Na^+ and Cl^- ions in water, and (c) the lubricant $\text{C}_{40}\text{H}_{82}$.

friction $\Gamma(x)$ associated with the pulling process. Using the constraint condition $x = x_0 + vt$ to change the integration variable from distance x to time t , we get

$$\Gamma(x) = \beta \int_0^{t(x)} d\tau \langle \delta f(t) \delta f(\tau) \rangle, \quad (6)$$

which can be directly calculated from the dcTMD simulations. In this way, $\langle W_{\text{diss}}(x) \rangle$ can be considered as dissipation correction of the work to give the correct free energy, hence the name “dcTMD”.

Notably, the assumption that the work distribution is well approximated by a Gaussian (in which case the above cumulant approximation is exact) is in principle the only condition underlying dcTMD, which might be an advantage compared to related approaches that calculate friction from pulling simulations [26–28]. While this supposition may be inapplicable to ligand-protein dissociation processes that provide several exit pathways of the ligand [29], we will show theoretically and numerically that the cumulant approximation is generally valid for fluid systems.

When we studied the enforced separation of various molecular systems [21, 29], we found that the friction calculated via Eq. (6) exhibits an intrinsic velocity dependence, whose origin is not apparent from the underlying Markovian Langevin model. To gain a microscopic understanding of these phenomena, here we extend the formal basis of dcTMD by deriving a generalized Langevin equation of the nonequilibrium pulling process [30–35]. This extension is essential to study the friction

in fluid systems, where pulled molecules and surrounding molecules are of the same size and weight, therefore impeding a timescale separation required for a Markovian description. In the Langevin framework, these non-Markovian effects are described via a two-time memory kernel $K(t, \tau)$ that can be directly calculated from dcTMD.

Considering various model fluids, from a simple Lennard-Jones liquid to the complex model lubricant $\text{C}_{40}\text{H}_{82}$ (Fig. 1), we show that the memory kernel may exhibit prominent non-Markovian behavior such as oscillatory features and a stretched-exponential decay. As most important effect we find, in a generalization of the observation that friction may be increased by position constraints [36], that underlying near-order effects decrease when the velocity of the pulled molecules approach the timescales of the bath. That is, both long-time tails of correlation functions and structural changes of the liquid may cause a velocity-dependence of the friction in fluids.

II. THEORY

A. Validation of the cumulant approximation

As explained above, the main assumption of dcTMD is that the distribution of the work W resembles a Gaussian to justify the cumulant approximation (2). A common reasoning for this claim invokes the limit of slow pulling velocities ($v \rightarrow 0$), where the system’s response is linear and the work is given as sum of many independent contributions in time [21, 24]. Extending the argument to independent contributions in space, here we show that for fluids a Gaussian work distribution arises as a consequence of the central limit theorem. Simply speaking, the proposition states that the sum of N independent random variables (with similar distribution) tends towards a normal distribution for large N [37].

To this end, we consider a fluid with $N + 2$ identical molecules and pull two molecules from their initial distance x_0 to a final distance x . In each pulling simulation, the applied constraint force f does work comprising the individual contributions W_i of the other N molecules,

$$W(\mathbf{q}_0) = \sum_{i=1}^N W_i, \quad (7)$$

where \mathbf{q}_0 denotes their initial condition. (While the work also depends on time and on the details of the MD force field, these dependencies are irrelevant for the reasoning here.) Since the initial conditions \mathbf{q}_0 are randomly sampled from equilibrium and the molecules are identical, the other N molecules have the same probability to scatter with the pulled molecules. Consequentially, the probability distribution of the work W_i is identical as well, such that $P(W_i) \sim P(W_j)$ for all molecules i, j .

Moreover most contributions W_i are statistically independent within the ensemble of trajectories, although within a particular trajectory the work contributions are not necessarily uncorrelated. These exceptions include molecules in the direct vicinity of the pulled particles, which may interact in a concerted manner and therefore result in non-independent work contributions. In contrast to independent scattering events, they involve at least three interaction partners, hence these correlations are presumably weak and may therefore still qualify for the central limit theorem [37]. This should apply to typical interactions described by a biomolecular force field at ambient conditions, but excludes fluids close to a critical point [38]. Hence the overall work W can be written as sum over N mostly independent random variables with similar distribution, which is just the requirement of the central limit theorem.

B. Definition of the friction factor

In previous work [21] we derived Eqs. (5) and (6) that define the dcTMD friction from a Markovian Langevin equation. However, the mere calculation of $\Gamma(x)$ does not require the presumption of a Langevin equation. To show this, we relate frictional forces f_{fric} and dissipative work W_{diss} via

$$f_{\text{fric}}(x) = -\frac{\partial \langle W_{\text{diss}} \rangle}{\partial x}, \quad (8)$$

which is valid since the frictional forces are on average the only source of dissipation. While this equation holds for any friction model, we can specifically apply it to Stokes friction, $f_{\text{fric}}(x) = -v\Gamma(x)$, which directly yields the position-dependent friction

$$\Gamma(x) := \frac{1}{v} \frac{\partial \langle W_{\text{diss}} \rangle}{\partial x}. \quad (9)$$

Note that this definition of $\Gamma(x)$ is general and does neither rely on a Langevin formalism nor requires a cumulant approximation. Rather by combining Eq. (9) with Jarzynski's identity, $\Delta G = -\beta^{-1} \ln \langle e^{-\beta W} \rangle$, we obtain the exact expression

$$\begin{aligned} \Gamma &= \frac{1}{v} \frac{\partial}{\partial x} (\langle W \rangle - \beta^{-1} \ln \langle e^{-\beta W} \rangle) \\ &= \frac{1}{v} \left(\langle f \rangle - \frac{\langle f e^{-\beta W} \rangle}{\langle e^{-\beta W} \rangle} \right) \\ &= \Gamma_{\text{cum}} - \frac{\beta^2 v^2}{2} \int_0^t dt_2 \int_0^t dt_1 \langle \delta f(t) \delta f(t_2) \delta f(t_1) \rangle + \text{h.o.t.}, \end{aligned} \quad (10)$$

where Γ_{cum} is given in Eq. (6). That is, any deviation from the cumulant approximation results in higher-order correlations of the constraint force contributing to the friction. Unfortunately, these higher-order terms (as well as the full Jarzynski's identity) are notoriously difficult to evaluate due to poor convergence behavior [24, 39].

C. Generalized Langevin equation

Given the validity of the cumulant approximation, we have shown above that the friction can be calculated from the two-time force autocorrelation function $\langle \delta f(t) \delta f(\tau) \rangle$. Interestingly, the absence of higher-order correlations also allows us to derive an exact generalized Langevin equation of the nonequilibrium process. It reads

$$m\ddot{x}(t) = -\frac{\partial G}{\partial x} - \int_0^t d\tau K(t, \tau) \dot{x}(\tau) + \eta(t) + f(t), \quad (11)$$

and comprises the mean force $-\partial G/\partial x$, a non-Markovian friction force with memory function $K(t, \tau)$, a stochastic force $\eta(t)$ due to the associated colored noise with zero mean, and the external pulling force $f(t)$.

To derive this equation, we partition the problem into system and bath, $H = H_S + H_B + H_{SB}$, where the system is $H_S(x, p) = p^2/2m + U(x)$, the bath $H_B(\mathbf{q})$ depends on phase-space coordinates \mathbf{q} , and the system-bath coupling is $H_{SB}(x, \mathbf{q})$. The free energy of the system is given by

$$\begin{aligned} G(x) &= -\beta^{-1} \ln \int d\mathbf{q} e^{-\beta[U(x) + H_{SB}(x, \mathbf{q})]} \\ &\equiv U(x) + U_{SB}(x). \end{aligned} \quad (12)$$

Adding the constraint force f , we use Hamilton's equation for the system to find

$$m\ddot{x} = -\frac{\partial G}{\partial x} + f_{SB}(x, \mathbf{q}) + f \quad (13)$$

with $f_{SB} = -\partial/\partial x (H_{SB} - U_{SB})$. Due to the constant velocity constraint, $x = x_0 + vt$, the total force vanishes, $m\ddot{x} = 0$, and we obtain the work to move the system from x_0 to x via an integration in time from 0 to t . Upon averaging over the bath, this yields

$$\Delta G = \langle W \rangle + v \int_0^t d\tau \langle f_{SB} \rangle, \quad (14)$$

where the last term is recognized as the dissipative work $\langle W_{\text{diss}} \rangle$. Assuming the validity of the cumulant approximation, moreover, we use Eqs. (5) and (6) to obtain

$$\int_0^t d\tau \langle f_{SB} \rangle = -\beta v \int_0^t dt_1 \int_0^{t_1} dt_2 \langle \delta f(t_2) \delta f(t_1) \rangle, \quad (15)$$

where we changed the integrated surface from a rectangle to a triangle to get an additional factor 2. By comparing the integrand on both sides and defining a fluctuating force via $\eta = f_{SB} - \langle f_{SB} \rangle$, we find

$$f_{SB}(x, \mathbf{q}) = -\beta v \int_0^t d\tau \langle \delta f(t) \delta f(\tau) \rangle + \eta \quad (16)$$

with $\langle \eta \rangle = 0$. Using $v = \dot{x}$, the insertion of Eq. (16) in Eq. (13) finally yields the desired generalized Langevin equation (11).

From the derivation we find that the memory kernel of the generalized Langevin equation is given by the auto-correlation function of the constraint force,

$$K(t_2, t_1) = \beta \langle \delta f(t_2) \delta f(t_1) \rangle. \quad (17)$$

Hence, dcTMD directly provides the two-time memory kernel accounting for the non-Markovian behavior of the nonequilibrium pulling process. This is remarkable, because multi-time memory functions of nonstationary processes are in general difficult to calculate [40, 41].

Since $\delta f = \eta$, we readily obtain the fluctuation dissipation theorem

$$\beta \langle \eta(t_2) \eta(t_1) \rangle = K(t_2, t_1), \quad (18)$$

which states that non-white noise η causes a finite decay time of the memory kernel K . Interestingly though, by using Eq. (6) in combination with $\dot{x}(\tau) = v$, Eq. (11) can be written in the form of a Markovian Langevin equation

$$m\ddot{x}(t) = -\frac{\partial G}{\partial x} - \Gamma(x)\dot{x} + \eta(t) + f(t) = 0. \quad (19)$$

although the noise is not delta-correlated due to Eq. (18).

Owing to the non-stationarity of the underlying process, $K(t_2, t_1)$ generally cannot solely be expressed as a function of the lag time $t_2 - t_1$. To nevertheless obtain a simple interpretation of the friction dynamics, we may average the force correlation function over a specific region in $x \in [x_1, x_2]$, where the resulting friction $\Gamma(x)$ varies only little. Using $\tau_i = (x_i - x_0)/v$ ($i = 1, 2$) to convert this spatial average to a time average, we obtain the one-time memory kernel

$$K(\tau) = \frac{\beta}{t_2 - t_1} \int_{t_1}^{t_2} dt \langle \delta f(t + \tau) \delta f(t) \rangle. \quad (20)$$

As will be demonstrated in Sec. IV, this averaged correlation function adequately illustrates the memory decay of the nonstationary process.

In the equilibrium limit of very slow pulling, we expect that the memory kernel (20) can be compared to the memory function obtained from an unbiased simulation. The latter can be calculated, e.g., by iteratively solving the Volterra equation [42]

$$m \langle \ddot{x}\ddot{x}(t) \rangle = K(t) \langle \dot{x}^2 \rangle + \int_0^t d\tau K(\tau) \langle \ddot{x}(t - \tau) \dot{x}(t) \rangle, \quad (21)$$

which can be derived from the generalized Langevin equation (11).

D. Velocity dependence of the friction

To focus on the velocity dependence of the friction, we may eliminate the inherent x -dependence by averaging

$\Gamma(x)$ over some pulling region $[x_1, x_2]$,

$$\widehat{\Gamma}(v) := \frac{1}{x_2 - x_1} \int_{x_1}^{x_2} dx' \Gamma(x') \quad (22)$$

$$= \frac{1}{v} \frac{\langle W_{\text{diss}}(x_2) \rangle - \langle W_{\text{diss}}(x_1) \rangle}{x_2 - x_1}, \quad (23)$$

where in the second line Eq. (9) was employed (see also Ref. 28). As in the definition of the memory kernel in Eq. (20), the averaging window is chosen to represent a characteristic region in x .

Since in dcTMD the friction Γ is completely determined by the force correlation function $\langle \delta f(t_2) \delta f(t_1) \rangle$, this function must also account for the dependence of the friction on the pulling velocity v . To study the origin of this effect, we first consider a simple single-exponential model

$$K(t_2, t_1) = \frac{\gamma}{\tau_C} e^{-|t_2 - t_1|/\tau_C} \quad (24)$$

with amplitude γ and correlation time τ_C . Pulling the system from x_0 to a fixed distance x for various velocities v , Eq. (6) yields the friction

$$\Gamma = \gamma \left(1 - e^{-v_C/v} \right), \quad (25)$$

where $v_C = (x - x_0)/\tau_C$. The velocity dependence is characterized by the ratio v_C/v , which relates the response rate of the bath to the velocity of the constrained particles. For low pulling velocities with $v_C/v \gg 1$, we find that $\Gamma = \gamma$. In the opposite case of high pulling velocities, the upper limit $t = (x - x_0)/v$ of the integral in Eq. (6) becomes shorter than the decay time τ_C of the autocorrelation function, such that the integral does not reach its maximum value. This reflects the fact that for a given pulling range $x - x_0$ the system is pulled too fast to access all dissipation channels present in the bath. The resulting velocity dependence is generic, in the sense that the effect occurs independent of the considered system as long as the pulling velocity is high enough.

When we average Eq. (25) over some pulling region $[x_0, x]$ as in Eq. (22), the averaged friction $\widehat{\Gamma}(v)$ also shows this generic behavior. Averaging over a region where Γ already converged to γ , we find $\widehat{\Gamma} = \gamma$. In general, on the other hand, we obtain

$$\widehat{\Gamma}(v) = \gamma \left(1 - \frac{v}{v_C} \left(1 - e^{-v_C/v} \right) \right), \quad (26)$$

which again depends on the pulling velocity.

We have also considered more complex forms of the autocorrelation function instead of Eq. (24), such as bi-exponential and stretched-exponential models reflecting the presence of multiple timescales of the bath [43]. While they too lead to explicit expressions for Γ and $\widehat{\Gamma}$ (see SI Methods), in essence they describe the same generic effect as discussed above. This indicates that more involved cases, such as a velocity dependence due to near-order effects, cannot be described by exponential models with constant amplitudes and decay times.

III. METHODS

All simulations were performed using Gromacs version 2016.3 [44], employing the implemented PULL code for dcTMD. Analysis of the dcTMD trajectories was carried out using our dcTMD Python package that is available at www.moldyn.uni-freiburg.de.

A. Lennard-Jones liquid.

The Lennard-Jones model consists of 800 argon atoms in a rectangular box of 3.4 nm width and periodic boundaries. Starting with a configuration in which two argon atoms exhibit a distance of $x = 0.35$ nm, we perform 10 ns of simulation with 1 fs time-step under NVT equilibrium conditions. We use the Bussi thermostat [45] at 80 K with a coupling time constant $\tau = 0.1$ ps, a van der Waals cut-off of 0.85 nm, and a distance constraint on x to obtain 10 000 equidistant system snapshots. These snapshots serve as starting configurations of 0.1 ns long NVT runs, which keep two tagged atoms at a fixed distance x , and employ redistributed velocities to generate an initial Boltzmann distribution for the subsequent nonequilibrium simulations. Pulling the two tagged atoms from $x = 0.35$ to 1.65 nm, we performed 5 000 dcTMD runs for velocities up to 0.005 nm/ps, and 10 000 runs for higher velocities. The dcTMD simulations were compared to a 1 ns long unbiased NVT equilibrium simulation with 10 fs resolution.

B. NaCl in water.

Extending the studies of Ref. 21, we performed NPT simulations using 893 water molecules plus a Na^+ and a Cl^- ion in a cubic box of 3 nm side length. Employing a 1 ns simulation of equilibration at fixed ion distance $x = 0.265$ nm, we generated 1000 starting points. After performing a 0.1 ns equilibration run for each point, we picked 10 frames of each run, each of which was again equilibrated for 10 ps assuming random velocities, to end up with in total 10 000 starting configurations. To obtain data for long ion distances, we pulled up to $x = 1.265$ nm using velocities $v = 0.0001, 0.001, 0.01$ and 0.1 nm/ps, and a time step of 1 fs. To better resolve velocity-dependent friction features, we employed additional pulling velocities, but pulled only until $x = 0.865$ nm. In this way, we simulated 1000 trajectories for velocities $v \leq 0.0005$ nm/ps, 5 000 for 0.001 nm/ps $\leq v \leq 0.006$ nm/ps, and 10 000 for higher velocities. We compared the dcTMD results to 50 unbiased simulations of 1 ns, writing out structural snapshots every 10 fs.

C. Lubricant $\text{C}_{40}\text{H}_{82}$.

All simulations are based on structures from Ref. 8 with 175 $\text{C}_{40}\text{H}_{82}$ molecules in a cuboid of size $5 \times 6.5 \times 8$ nm³ and periodic boundary conditions. Force field parameters were generated using antechamber [46] and acpype [47], employing OPLS-AA atom types [48] and AM1/BCC charges [49, 50]. The structures were minimized using steepest descend. Equilibration was performed in the NVT ensemble for 5 ns (1 fs time step), using the Bussi thermostat at 600 K ($\tau = 0.2$ ps). For Coulomb interactions, we used the Particle Mesh Ewald summation method [51] with a real-space cut-off of 1.3 nm, and a van der Waals cut-off of 1.3 nm. Production runs consisted of one NVT run of 100 ns to generate initial configurations for the subsequent pulling simulations. Starting from 1000 initial configurations, two hydrocarbons at a center-of-mass distance $x_0 \approx 0.6$ nm were picked as tagged particles. After pulling to the exact position if necessary, the systems were again equilibrated with fixed x for 100 ps. Using a pulling range from $x = 0.6$ to 2.1 nm, the resulting configurations were used as starting conditions for the following dcTMD simulations: 200 runs for $v \leq 0.00075$ nm/ps, 500 runs for 0.0015 nm/ps $\leq v \leq 0.005$ nm/ps, and 1000 runs for higher velocities. Moreover, we performed an 1 ns-long unbiased simulation using a 1 fs resolution.

D. Computation of friction and memory kernels.

As described above, we perform for each system and pulling velocity a number of nonequilibrium dcTMD simulations, from each of which we record the constraint forces $f(t)$ at a temporal resolution of 1 fs. By integrating f via the trapezoidal rule, we calculate the work W and its mean $\langle W \rangle$ and variance $\langle \delta W^2 \rangle$ for all considered distances x , which yields the free energy profile $\Delta G(x)$ and the dissipated work $W_{\text{diss}}(x)$ via Eq. (2).

By numerical differentiation of $\langle W_{\text{diss}}(x) \rangle$, we then calculate the friction profile $\Gamma(x)$ via Eq. (9). Since the derivative is prone to large fluctuations, we employ an averaging window Δx , using $\Delta x = 0.026$ nm for the Lennard-Jones model, 0.02 nm for NaCl and 0.15 nm for $\text{C}_{40}\text{H}_{82}$. In this way, fluctuations are minimized, while main features of the friction profile are still resolved. While the free energy ΔG is given as the difference of two large numbers in dcTMD [Eq. (2)], the friction Γ can be directly obtained from $\langle W_{\text{diss}}(x) \rangle$ and is therefore less prone to statistical errors than ΔG in the trajectory average.

As additional test of the cumulant approximation, we also calculated $\hat{\Gamma}$ directly via Jarzynski's identity [Eq. (10)]. While cumulant and Jarzynski results agree well in general (Fig. S1), for large velocities we still find well-known convergence issues of Jarzynski's identity [24, 39].

The dcTMD memory kernel $K(t)$ is directly computed

from the constraint force trajectories $\delta f(t)$ according to Eq. (20). To study the generic onset of the friction discussed in Eq. (25), it is instructive to integrate the memory kernel, $\gamma(t) = \int_0^t d\tau K(\tau)$, and consider the convergence of $\gamma(t)$ for various pulling velocities (Fig. S2).

To compare the dcTMD results to the equilibrium memory kernel obtained from unbiased simulations, we iteratively solved Eq. (21) for $K(t)$ as described in Ref. 42. As this requires the accurate calculation of velocities and forces by finite differences, we used a short time step of 10 fs for the Lennard-Jones model and NaCl and 1 fs for $C_{40}H_{82}$. Using a 10 fs time step, we had to correct for the artificial force spike at $t = 0$ by employing a parabolic fit to the subsequent time frames. Moreover, since the estimator may fail at the long-time tail of the memory kernel, we performed a fit of the tail to correct for the noise and to extrapolate at longer times. That is, for the Lennard-Jones model we fit a mono-exponential function to the results obtained for 0.8 – 1.4 ps, in order to extend the kernel from 1.4 ps onward. For NaCl we performed an exponential fit from 0.4 to 2.0 ps to connect at 0.5 ps, and for $C_{40}H_{82}$ we used a stretched-exponential fit from 2.2 to 20 ps to continue from 10 ps.

IV. RESULTS AND DISCUSSION

A. Friction and memory of a Lennard-Jones liquid.

To demonstrate how dcTMD works in practice, we start with a Lennard-Jones liquid as a system of minimal microscopic complexity. The idea is to pull apart two tagged Lennard-Jones particles, which results in a partitioning into a “system” of two spheres that are embedded in a “bath” consisting of the remaining particles (Fig. 1a). Since the constrained particles are of the same size and weight as the bath particles, the model challenges the ansatz of a Markovian Langevin equation employed in the original formulation of dcTMD [21], but should be well represented by the generalized Langevin equation [Eq. (11)]. As the main assumption of dcTMD is a Gaussian work distribution $P(W)$ to justify Eq. (2), we first show in Fig. 2a that this is indeed the case for all considered pulling velocities v . Comparing $P(W)$ directly to the corresponding normal distribution (Fig. S3a), we only find deviations at the poorly sampled tails ($|W| \gtrsim 3\sigma$) of the distribution. Moreover, we checked that dcTMD reproduces the well-known radial distribution function and corresponding free energy profile of a Lennard-Jones liquid for velocities up to 0.01 nm/ps (Fig. S3b).

We are now in a position to discuss the friction properties of the Lennard-Jones liquid, see Fig. 2. To represent the magnitude of the friction in terms of a damping rate with unit 1/ps, in all figures we divided the friction by the reduced mass m of the considered system. Depicted as a function of the position, the friction $\Gamma(x)$ defined in Eq. (9) starts at $\Gamma(x_0 = 0.35 \text{ nm}) = 0$. The initial steep

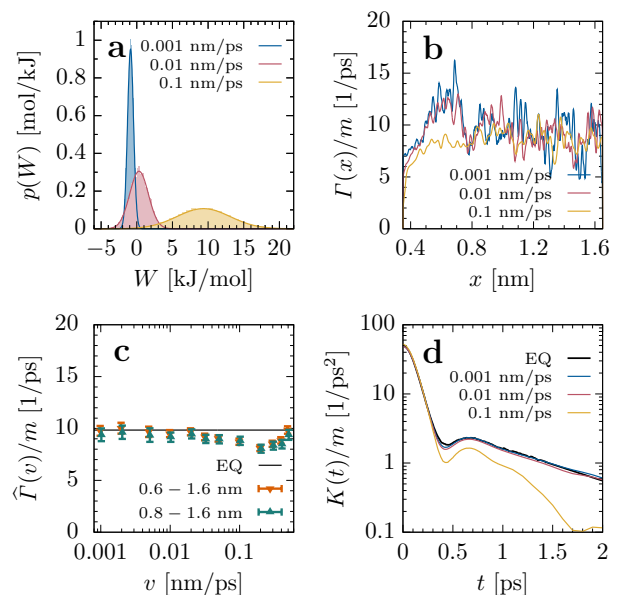


FIG. 2. Characterization of the friction of a Lennard-Jones liquid as obtained from dcTMD simulations using various pulling velocities v . (a) Distribution of the work W performed on the system, (b) position-dependent friction $\Gamma(x)$ [Eq. (9)], (c) position-averaged friction $\hat{\Gamma}(v)$ [Eq. (22)] evaluated for two averaging windows with error bars corresponding to a bootstrap estimate of the 95% confidence interval, and (d) friction memory kernel [Eq. (20)]. EQ indicates equilibrium results obtained from unbiased MD simulations.

rise of $\Gamma(x)$ reflects the generic onset of the friction discussed in Eq. (25). While this effect becomes more important with increasing velocity, $\Gamma(x)$ already plateaus for $x \approx 0.5 \text{ nm}$ even for 0.1 nm/ps, meaning that this type of velocity dependence is not relevant here. For long inter-particle distances, $x \gtrsim 0.8 \text{ nm}$, the friction is found to fluctuate around a roughly constant value.

As an unexpected feature, we note a significant maximum of $\Gamma(x)$ at $x \approx 0.6 \text{ nm}$ for small velocities. This is a consequence of the fact that this distance is just large enough for a third particle to shortly interact with both pulled particles. As can be seen from the particle distribution around the pulled particles (Fig. S3c), the structural arrangement is similar to a small cluster of crystallized Lennard-Jones spheres. Caused by pulling-induced suppression of fluctuations of the constrained particles, the effect does not occur in the bulk liquid [36]. Thus, if x is changed slowly enough, interactions with the bath may take place that would not occur in the unconstrained case.

To further study the velocity dependence of the friction, we next consider the position-averaged friction $\hat{\Gamma}(v)$ [Eq. (22)] shown in Fig. 2c. Performing averages with and without including the maximum of $\Gamma(x)$ around $x = 0.6 \text{ nm}$ is found to hardly change $\hat{\Gamma}(v)$. Rather we see that overall the $\hat{\Gamma}(v)$ is well approximated by its equilibrium value calculated from Eq. (21). Starting

with $v = 0.01$ nm/ps, however, we observe a small gradual decrease of the friction up to $v = 0.2$ nm/ps, where the probe particles approach the mean thermal velocity $\langle v \rangle = \sqrt{8k_B T / (\pi m)} \approx 0.29$ nm/ps. That is, the pulled particles experience less drag if they move with similar speed as the surrounding particles, thus minimizing the collisions with the environment. The effect vanishes for even larger pulling velocities, when the constrained particles move faster than the average bath velocity.

As system and bath particles are identical and therefore do not exhibit a timescale separation, it is interesting to study the memory kernel $K(t)$ that reports on the resulting non-Markovian behavior. We first discuss the equilibrium friction kernel, which was calculated from an unbiased simulation using Eq. (21). As shown in Fig. 2d, $K(t)$ undergoes a rapid initial decay leading to a recurrence at $t = 0.6$ ps, before it decreases exponentially on a timescale of ≈ 1 ps. Here the initial decay and the recurrence account for the interaction of two colliding particles with an average interaction time of ≈ 0.6 ps, while the long-time decay reflects the average time between two scattering events. We note that a phenomenological bi-exponential ansatz of the memory kernel (in the spirit of Eq. (24)) would qualitatively reproduce these results, with the exception of the recurrence which reflects the microscopic collision process.

Comparing the equilibrium friction kernel to the nonequilibrium results obtained from dcTMD [Eq. (20)], Fig. 2d reveals almost perfect agreement of equilibrium and dcTMD results for velocities up to 0.01 nm/ps. For $v = 0.1$ nm/ps, on the other hand, the dcTMD memory kernel decays significantly faster compared to the equilibrium kernel, which is in line with the decrease of $\hat{\Gamma}(v)$ in Fig. 2c. Evidently, the latter behavior cannot be reproduced with a bi-exponential memory kernel with constant decay times.

B. Dissociation of NaCl in water

The enforced ion dissociation of NaCl in water can be viewed as an idealized microrheological experiment that probes the interactions experienced by the ions [3]. While we still consider only two particles, the situation turns out to be much more complex than a Lennard-Jones model, which is because of the electrostatic interaction between the Na^+ and Cl^- ions and the structured and dynamical water environment. This is already evident from the free energy profile $\Delta G(x)$ along the interionic distance x (Fig. 3a), whose first maximum at $x \approx 0.4$ nm corresponds to the binding-unbinding transition of the two ions, while the second smaller maximum at $x \approx 0.6$ nm reflects the transition from a common to two separate hydration shells [52]. As the enforced separation of the ions again results in a Gaussian work distribution for all considered pulling velocities (Fig. S4a,b), the supposedly complex friction behavior of solvated NaCl is nevertheless amenable to dcTMD mod-

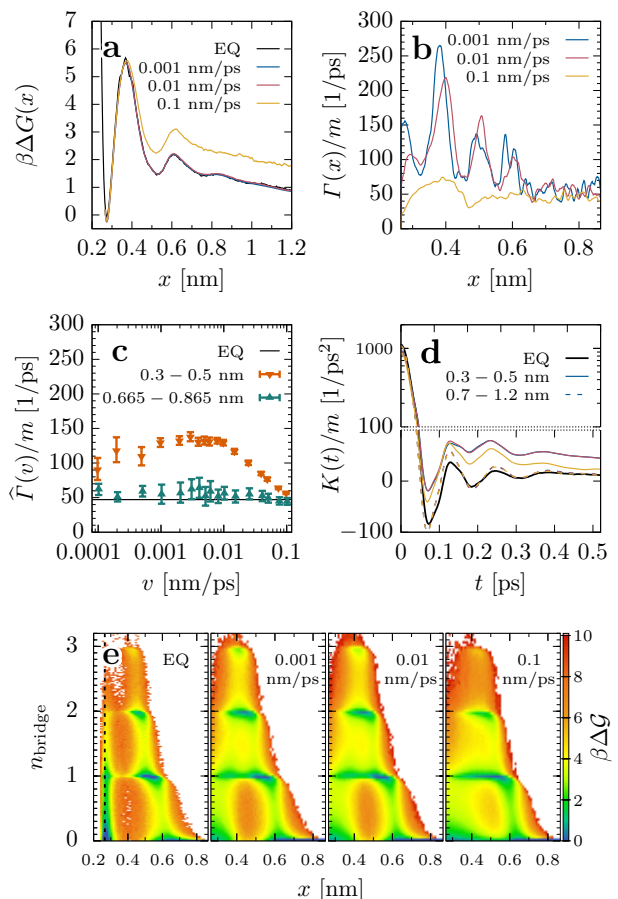


FIG. 3. Complex friction behavior of NaCl in water. Shown are (a) free energy $\Delta G(x)$ and (b) friction profiles $\Gamma(x)$ as a function of the interionic distance x , (c) position-averaged friction $\hat{\Gamma}(v)$ evaluated for two averaging windows with error bars corresponding to a bootstrap estimate of the 95% confidence interval, and (d) associated friction memory kernels which are depicted on a logarithmic scale for $K/m \geq 100/\text{ps}^2$ and on a linear scale otherwise. Color code is as in (b). (e) Probability distribution that the ions at distance x are connected via n water molecules.

eling.

Figure 3b shows the resulting friction profile $\Gamma(x)$ for various pulling velocities, which is indeed quite structured in the region of the two solvation shells ($x \lesssim 0.7$ nm), where the maxima at 0.39 and 0.59 nm correlate well with the maxima found for $\Delta G(x)$. Hence these features are associated with the formation of hydration shells shared between the ions [21], which can also be seen in two-dimensional density plots of the system (Fig. S4c). As for the Lennard-Jones model (Fig. 2b), the structural features vanish for larger pulling velocities. Moreover, the generic onset of the friction [Eq. (25)] again does not play a major role, as $\Gamma(x)$ reaches a plateau for ≈ 0.4 nm even at the highest considered velocity ($v = 0.1$ nm/ps). For distances larger than 0.7 nm, $\Gamma(x)$ converges to a common value for all velocities. Here, the friction is dom-

inated by collisions of the ions with water molecules from their own hydration shells [21].

Because of the large difference of $\Gamma(x)$ for small ($0.3 \text{ nm} \leq x \leq 0.5 \text{ nm}$) and large ($0.665 \text{ nm} \leq x \leq 0.865 \text{ nm}$) distances, it is instructive to separately consider these two averaging windows when we study the velocity dependence of the averaged friction $\hat{\Gamma}(v)$ (Fig. 3c). As expected from Fig. 3b, we find that for large distances $\hat{\Gamma}(v)$ is constant, and in fact coincides well with its equilibrium value calculated from Eq. (21). For short distances, on the other hand, we find a significant velocity dependence, i.e., the friction is enhanced by up to a factor 3 for moderate velocities ($v \lesssim 0.01 \text{ nm/ps}$) and decreases to its equilibrium value for higher velocities. Similar to the Lennard-Jones liquid, the enhancement is caused by constraint-induced fluctuations that do not occur at equilibrium. (Indeed, unconstrained calculations of $\Gamma(x)$ revealed a structureless friction profile [53].) Also similarly, the friction decreases when the pulling approaches the picosecond timescale of the reordering of the solvation shells, causing the ions to experience less drag. In contrast to the Lennard-Jones model, however, these effects are much larger (factor 3 vs. 1.2) for the water-solvated ion system.

The above finding of a velocity-dependent reordering of common ion hydration shells can be nicely illustrated by considering the probability distribution that the ions at distance x are connected via $n = 0, 1, 2, 3$ water molecules (Fig. 3e) [52, 54]. In the unbiased case, we find typically zero to one bridging water molecules at the minimum ($x \approx 0.28 \text{ nm}$), while up to three bridging waters are found during dissociation or association ($x \approx 0.35 \text{ nm}$). For the constrained distribution [55], we indeed observe a bias towards a higher number of connecting water molecules than present in the unbiased case, indicating altered dynamics within the hydration shells. For fast pulling velocities, the number of bridging water molecules again gradually becomes smaller – up to a point, where an absence of bridging water molecules during the transition becomes viable as well.

As the Na^+ and Cl^- ions and the surrounding water molecules are of similar mass and thus move on a similar timescale, we again expect non-Markovian behavior of the system. Figure 3d shows the corresponding friction memory kernel obtained from unbiased equilibrium simulations and dcTMD simulations. In the equilibrium case, the memory kernel exhibits a rapid ($\approx 25 \text{ fs}$) initial decay, which is followed by oscillatory features with a period of $\approx 120 \text{ fs}$, that are damped on a 1 ps timescale. While the initial decay reflects the timescale of direct ion-water collisions [21], the long-time decay of the kernel agrees well with the average lifetime (0.77 ps) of a water molecule in an ion hydration shell (Fig. S4d). As discussed in Ref. 41, the oscillatory features correspond to damped ion-water oscillations.

When using dcTMD to calculate the memory kernel for finite pulling velocities, we again consider averaging windows for short and long distances [Eq. (20)]. In the latter

case, the dcTMD kernel closely recovers the unbiased results for all velocities. Considering short distances, on the other hand, the amplitude of the long-time decay is significantly increased, which again is a consequence of the above discussed reordering of the solvation shells. A similar effect was observed for the interaction of constrained van der Waals particles within bulk water [36].

C. Friction and long-time memory of $\text{C}_{40}\text{H}_{82}$

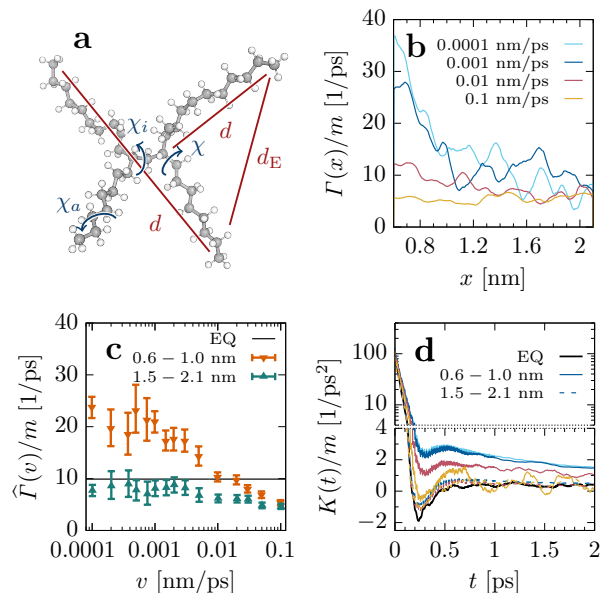


FIG. 4. Friction of a hydrocarbon lubricant. (a) Structure of $\text{C}_{40}\text{H}_{82}$, indicating various inter-atom distances d_j and backbone dihedral angles χ_j . (b) Friction profiles $\Gamma(x)$ as a function of the center-of-mass distance x , obtained for various pulling velocities v . (c) Position-averaged friction $\hat{\Gamma}(v)$ evaluated for two averaging windows. Error bars correspond to a bootstrap estimate of the 95% confidence interval. (d) Memory kernel $K(t)$, shown on a logarithmic scale for $K/m \geq 4 \text{ ps}^{-2}$ and on a linear scale otherwise. Color code is as in (b).

The hydrocarbon $\text{C}_{40}\text{H}_{82}$ represents a model lubricant with a well-established shear-velocity dependence [8]. To probe the friction and its dependence on velocity, we pull two tagged $\text{C}_{40}\text{H}_{82}$ molecules apart along their centers of mass. Due to their four-armed starfish-like structure (Fig. 4a) and relatively dense packing (Fig. 1c), the tagged and surrounding alkane molecules interact in a vastly complex, intertwined fashion. While we may expect an intricate behavior of the friction and the memory kernel, pulling simulations again yield a Gaussian work distribution (Fig. S5a,b) which facilitates a dcTMD analysis.

The dcTMD friction profile $\Gamma(x)$ shown in Fig. 4b exhibits a clear position and velocity dependence. While the data are more noisy than for the simpler systems

discussed above, we again find for slow velocities that the friction is higher at short distances, while at large distances the slow-velocity friction approaches the high-velocity results. Accordingly, when averaged over short distances, the friction $\hat{\Gamma}(v)$ decreases with increasing velocity (Fig. 4c). When averaged over long distances, on the other hand, $\hat{\Gamma}(v)$ remains roughly constant and close to its equilibrium value up to ≈ 0.003 nm/ps, from where it starts to drop slightly. Since the arms of the two pulled alkane molecules can be in contact even for a center-of-mass distance of 2.0 nm, this velocity dependence at long distances may either be attributed to remaining direct interactions or to near-ordering effects as found for the other two systems. In fact, nonequilibrium MD simulations of similar systems revealed an overall alignment of the lubricants along the shearing direction, which also results in a decreased radius of gyration[7, 8]. Unlike to the simpler systems, $C_{40}H_{82}$ moreover exhibits a generic velocity dependence [Eq. (25)], because the underlying friction memory kernel decays too slow to be completely integrated by fast pulling velocities (Fig. S2).

To discuss the rather complex behavior of this memory kernel $K(t)$ shown in Fig. 4d, we first focus on the equilibrium results for $K(t)$. Initially the kernel exhibits a decay until ≈ 0.2 ps, which corresponds to thermal motions and collisions of the two constrained molecules. Following a recurrence at $t \approx 0.5$ ps, the kernel shows a slow decay, which is best fitted to a stretched-exponential function ($\sim e^{-(t/\tau)^\alpha}$ with $\alpha \approx 0.2$). To obtain dcTMD results, we again averaged the memory kernel over either short or long distances [Eq. (20)]. While in the latter case the dcTMD kernel closely recovers the equilibrium results for all velocities, short distances result in an significant increase of the amplitude of the long-time decay for slow velocities, which is the main origin of the velocity dependence of $\hat{\Gamma}(v)$ in Fig. 4c.

While a mono-exponential long-time decay of the memory kernel found for the simpler systems suggests a single main timescale of the bath, the stretched exponential form of $K(t)$ in Fig. 4d is indicative of bath dynamics on a multitude of timescales [43]. To elucidate the underlying microscopic mechanism, it is instructive to illustrate the motion of $C_{40}H_{82}$ along representative internal coordinates as indicated in Fig. 4a. When we calculate the equilibrium autocorrelation function of these coordinates, we find that motions involving a single arm of $C_{40}H_{82}$, such as the dihedral angle χ_a or the distance d_I , decay on a picosecond timescale (Fig. S5e,f). Distances connecting the ends of two arms such as d_A and d_E , are found to decay on tens of picosecond, while the internal rotation of one or two arms described by dihedral angles χ_C and χ_i takes about 100 ps (Fig. S5e,f). Hence it is the combination of the above described bath motions occurring on timescales across three orders of magnitude that yield the stretched exponential long-time decay of the memory kernel.

V. CONCLUSIONS

To gain a microscopic understanding of the phenomena leading to velocity-dependent friction in fluids, we have employed dissipation-corrected targeted molecular dynamics (dcTMD), which pulls apart two tagged molecules (the “system”) in the presence of the surrounding molecules (the “bath”). Since system and bath particles are identical in fluids and therefore do not exhibit a timescale separation, we have extended the theoretical framework of dcTMD to account for the resulting non-Markovian behavior of the system. dcTMD was shown to directly provide the nonequilibrium memory kernel $K(t_2, t_1)$ [Eq. (17)], from which the mean dissipated work $\langle W_{\text{diss}}(x) \rangle$ and the associated friction profile $\Gamma(x)$ along the pulling path x [Eq. (9)] is readily calculated. Moreover, we have shown that the nonstationary kernel $K(t_2, t_1)$ can be related to an equilibrium memory kernel $K(t)$ [Eq. (20)], and compared this result to a kernel obtained from a Volterra equation derived from unbiased simulations. Because dcTMD rests on the assumption that the distribution of the work W is well approximated by a Gaussian (to justify the cumulant approximation in Eq. (2)), we have validated this condition for all considered fluids and pulling velocities. As a consequence, the nonequilibrium process is completely described by a two-time autocorrelation function and thus exactly modeled by a generalized Langevin equation (11). As the cumulant approximation represents the only assumption underlying dcTMD, this result is remarkable because it suggests that dcTMD should be a valuable approach to characterize the friction behavior of even complex fluids.

Considering three fluids, from a simple Lennard-Jones liquid, via solvated NaCl to the complex lubricant $C_{40}H_{82}$, we have identified near-order structural effects as main reason for the apparent velocity dependence of the friction for all systems. It starts with the observation that the friction experienced by position-constrained molecules generally increases compared to unconstrained molecules [36]. This effect typically occurs at short distances of the two constrained molecules, where the molecules either interact directly or via the surrounding molecules. At long distances, these interactions vanish and the friction decreases to its equilibrium value. Being pulled apart with slow velocity, the molecules therefore experience enhanced friction as long as these near-order effects prevail. In a similar vein, perturbation of local structures around a pulled probe has been linked to the onset of shear thinning in a theoretical study on microrheology [56]. In the case of high pulling velocity similar to the speed of the surrounding particles, the particles experience less drag, because they minimize the collisions with the environment.

Although the above described mechanism is similar for all considered systems, the resulting effect on the friction differs significantly, reflecting the quite different near-order effects of the fluids. While the friction in a

short-range Lennard-Jones liquid hardly depends on the pulling velocity at all (Fig. 2), the well-defined hydration shells of Na^+ and Cl^- ions in water give rise to a very structured friction profile $\Gamma(x)$ and a short-distant enhancement of the friction by a factor 3 (Fig. 3). The four-armed lubricant $\text{C}_{40}\text{H}_{82}$, on the other hand, may exhibit direct interactions of the two pulled alkanes up to 2 nm, which enhances the friction by a factor 2 at low velocities (Fig. 4). As another effect of the numerous internal degrees of freedom of $\text{C}_{40}\text{H}_{82}$ undergoing conformational dynamics on multiple timescales, we have identified a stretched exponential long-time decay of the friction memory kernel. Indeed, the timescales of the conformational dynamics of polymer chains have been linked to shear thinning [6], with fast shearing leading to disentanglement of side chains and decreasing fluid internal friction [9]. Since the kernel decays too slow to be completely sampled by fast pulling velocities, the lubricant moreover exhibits a generic velocity dependence as discussed by Eq. (25). These findings are in line with microrheological experiments that suggest a connection between the time scales of external driving and the equilibrium relaxation time of a fluid for the onset of non-Newtonian friction [57].

In summary, we have found that both long-time tails of correlation functions and structural changes of the liquid may cause the velocity-dependence of the friction in fluids. While previous experimental and theoretical investigations proposed either of these effects as the cause for non-Newtonian friction in selected fluids, we have demonstrated that both effects are a general feature of fluids independent of its internal complexity.

ACKNOWLEDGMENTS

We thank Kerstin Falk and Benjamin Lickert for numerous instructive and helpful discussions. This work has been supported by the Deutsche Forschungsgemeinschaft (DFG) via the Research Unit FOR 5099 "Reducing complexity of nonequilibrium" (project No. 431945604). The authors acknowledge support by the bwUniCluster computing initiative, the High Performance and Cloud Computing Group at the Zentrum für Datenverarbeitung of the University of Tübingen, and the Rechenzentrum of the University of Freiburg, the state of Baden-Württemberg through bwHPC and the DFG through grants No. INST 37/935-1 FUGG and No. INST 39/963-1 FUGG.

-
- [1] Denis J. Evans and Gary P. Morriss, *Statistical Mechanics of Nonequilibrium Liquids* (Cambridge University, 2007).
- [2] Daniel T.N. Chen, Qi Wen, Paul A. Janmey, John C. Crocker, and Arjun G. Yodh, "Rheology of soft materials," *Annu. Rev. Condens. Matter Phys.* **1**, 301–322 (2010).
- [3] E. M. Furst and T. M. Squires, *Microrheology* (Oxford University, 2021).
- [4] Xiang Cheng, Jonathan H. McCoy, Jacob N. Israelachvili, and Itai Cohen, "Imaging the Microscopic Structure of Shear Thinning and Thickening Colloidal Suspensions," *Science* **333**, 1276–1279 (2011).
- [5] Scott S Bair, *High Pressure Rheology for Quantitative Elastohydrodynamics* (Elsevier, 2019).
- [6] Benjamin Huber, Markus Harasim, Bernhard Wunderlich, Martin Kroeger, and Andreas R Bausch, "Microscopic origin of the non-Newtonian viscosity of semiflexible polymer solutions in the semidilute regime," *ACS Macro Lett.* **3**, 136–140 (2014).
- [7] Pinzhi Liu, Jie Lu, Hualong Yu, Ning Ren, Frances E. Lockwood, and Q. Jane Wang, "Lubricant shear thinning behavior correlated with variation of radius of gyration via molecular dynamics simulations," *J. Chem. Phys.* **147**, 084904 (2017).
- [8] Kerstin Falk, Daniele Savio, and Michael Moseler, "Nonempirical free volume viscosity model for alkane lubricants under severe pressures," *Phys. Rev. Lett.* **124**, 105501 (2020).
- [9] Ranajay Datta, Leonid Yelash, Friederike Schmid, Florian Kummer, Martin Oberlack, Mária Lukáčová-Medvid'ová, and Peter Virnau, "Shear-thinning in oligomer melts-molecular origins and applications," *Polymers* **13**, 2806 (2021).
- [10] Xinliang Xu, Stuart A. Rice, and Aaron R. Dinner, "Relation between ordering and shear thinning in colloidal suspensions," *Proc. Natl. Acad. Sci. USA* **110**, 3771–3776 (2013).
- [11] Claire A. Lemarchand, Nicholas P. Bailey, Billy D. Todd, Peter J. Daivis, and Jesper S. Hansen, "Non-Newtonian behavior and molecular structure of Coee bitumen under shear flow: A non-equilibrium molecular dynamics study," *J. Chem. Phys.* **142** (2015), 10.1063/1.4922831.
- [12] Moumita Maiti, Annette Zippelius, and Claus Heussinger, "Friction-induced shear thickening: A microscopic perspective," *Europhys Lett.* **115**, 54006 (2016).
- [13] Harold A. Scheraga, "Non-Newtonian viscosity of solutions of ellipsoidal particles," *J. Chem. Phys.* **23**, 1526 (1955).
- [14] R. Vogelsang and C. Hoheisel, "Determination of the friction coefficient via the force autocorrelation function. A molecular dynamics investigation for a dense Lennard-Jones fluid," *J. Stat. Phys.* **47**, 193–207 (1987).
- [15] John E Straub, Bruce J Berne, and Benoît Roux, "Spatial dependence of time-dependent friction for pair diffusion in a simple fluid," *J. Chem. Phys.* **93**, 6804–6812 (1990).
- [16] Matthias Fuchs and Michael E. Cates, "Schematic models for dynamic yielding of sheared colloidal glasses," *Faraday Discuss.* **123**, 267–286 (2003).
- [17] G. Hummer, "Position-dependent diffusion coefficients and free energies from Bayesian analysis of equilibrium and replica molecular dynamics simulations," *New J. Phys.* **7**, 34 (2005).

- [18] Ignacia Echeverria, Dmitrii E. Makarov, and Garegin A. Papoian, “Concerted dihedral rotations give rise to internal friction in unfolded proteins,” *J. Am. Chem. Soc.* **136**, 8708–8713 (2014).
- [19] A. V. Straube, B. G. Kowalik, R. R. Netz, and F. Höfling, “Rapid onset of molecular friction in liquids bridging between the atomistic and hydrodynamic pictures,” *Commun. Phys.* **3**, 1–11 (2020).
- [20] Martin Müser, “Velocity dependence of kinetic friction in the Prandtl-Tomlinson model,” *Phys. Rev. B* **84**, 125419 (2011).
- [21] Steffen Wolf and G. Stock, “Targeted molecular dynamics calculations of free energy profiles using a nonequilibrium friction correction,” *J. Chem. Theory Comput.* **14**, 6175–6182 (2018).
- [22] J. Schlitter, M. Engels, and P. Krüger, “Targeted molecular dynamics - a new approach for searching pathways of conformational transitions,” *J. Mol. Graph.* **12**, 84–89 (1994).
- [23] C. Jarzynski, “Nonequilibrium equality for free energy differences,” *Phys. Rev. Lett.* **78**, 2690–2693 (1997).
- [24] D A Hendrix and C Jarzynski, “A “fast growth” method of computing free energy differences,” *J. Chem. Phys.* **114**, 5974 (2001).
- [25] Christoph Dellago and Gerhard Hummer, “Computing equilibrium free energies using non-equilibrium molecular dynamics,” *Entropy* **16**, 41–61 (2014).
- [26] S. Park and K. Schulten, “Calculating potentials of mean force from steered molecular dynamics simulations,” *J. Chem. Phys.* **120**, 5946–5961 (2004).
- [27] Julius C. F. Schulz, Markus S. Miettinen, and R. R. Netz, “Unfolding and folding internal friction of β -hairpins is smaller than that of α -helices,” *J. Phys. Chem. B* **119**, 4565–4574 (2015).
- [28] R. Kailasham, Rajarshi Chakrabarti, and J. Ravi Prakash, “Wet and dry internal friction can be measured with the Jarzynski equality,” *Phys. Rev. Research* **2**, 013331 (2020).
- [29] Steffen Wolf, Benjamin Lickert, Simon Bray, and Gerhard Stock, “Multisecond ligand dissociation dynamics from atomistic simulations,” *Nat. Commun.* **11**, 2918 (2020).
- [30] Robert Zwanzig, *Nonequilibrium Statistical Mechanics* (Oxford University, Oxford, 2001).
- [31] Shinnosuke Kawai and Tamiki Komatsuzaki, “Derivation of the generalized Langevin equation in nonstationary environments,” *J. Chem. Phys.* **134**, 114523 (2011).
- [32] Hugues Meyer, Thomas Voigtmann, and Tanja Schilling, “On the non-stationary generalized Langevin equation,” *J. Chem. Phys.* **147**, 214110 (2017).
- [33] Bingyu Cui and Alessio Zaccone, “Generalized Langevin equation and fluctuation-dissipation theorem for particle-bath systems in external oscillating fields,” *Phys. Rev. E* **97**, 060102 (2018).
- [34] Benjamin Lickert, S. Wolf, and Gerhard Stock, “Data-driven Langevin modeling of nonequilibrium processes,” *J. Phys. Chem. B* **125**, 8125–8136 (2021).
- [35] Tanja Schilling, “Coarse-grained modelling out of equilibrium,” arxiv.org/abs/2107.09972 (2021).
- [36] Jan O. Daldrop, Bartosz G. Kowalik, and Roland R. Netz, “External potential modifies friction of molecular solutes in water,” *Phys. Rev. X* **7**, 041065 (2017).
- [37] P. Billingsley, *Probability and Measure* (Wiley, 1995).
- [38] D. Sornette, *Critical Phenomena in Natural Sciences* (Springer, 2006).
- [39] Gerhard Hummer, “Fast-growth thermodynamic integration: Error and efficiency analysis,” *J. Phys. Chem.* **114**, 7330–7337 (2001).
- [40] Gerhard Jung, Martin Hanke, and Friederike Schmid, “Iterative reconstruction of memory kernels,” *J. Chem. Theory Comput.* **13**, 2481–2488 (2017).
- [41] Hugues Meyer, Steffen Wolf, Gerhard Stock, and Tanja Schilling, “A numerical procedure to evaluate memory effects in non-equilibrium coarse-grained models,” *Adv. Theory Simul.* **111**, 2000197 (2020).
- [42] Hyun Kyung Shin, Changho Kim, Peter Talkner, and Eok Kyun Lee, “Brownian motion from molecular dynamics,” *Chem. Phys.* **375**, 316–326 (2010).
- [43] Peter Hamm, Jan Helbing, and Jens Bredenbeck, “Stretched versus compressed exponential kinetics in α -helix folding,” *Chem. Phys.* **323**, 54–65 (2006).
- [44] Mark James Abraham, Teemu Murtola, Roland Schulz, Szilard Pall, Jeremy C. Smith, Berk Hess, and Erik Lindahl, “Gromacs: High performance molecular simulations through multi-level parallelism from laptops to supercomputers,” *SoftwareX* **1**, 19–25 (2015).
- [45] Giovanni Bussi and Michele Parrinello, “Accurate sampling using Langevin dynamics,” *Phys. Rev. E* **75**, 056707 (2007).
- [46] Junmei Wang, Wei Wang, Peter A Kollman, and David A Case, “Automatic atom type and bond type perception in molecular mechanical calculations,” *J. Mol. Graph. Model.* **25**, 247–260 (2006).
- [47] Alan W. Sousa da Silva and Wim F. Vranken, “ACPYPE - AnteChamber PYthon Parser interfacE,” *BMC Res. Notes* **5**, 367 (2012).
- [48] Leela S. Dodda, Israel Cabeza de Vaca, Julian Tirado-Rives, and William L. Jorgensen, “LigParGen web server: an automatic OPLS-AA parameter generator for organic ligands,” *Nucleic Acids Res.* **45**, W331–W336 (2017).
- [49] A. Jakalian, B. L. Bush, D. B. Jack, and C. I. Bayly, “Fast, efficient generation of high-quality atomic Charges. AM1-BCC model: I. Method,” *J. Comput. Chem.* **21**, 132–146 (2000).
- [50] Araz Jakalian, David B Jack, and Christopher I Bayly, “Fast, efficient generation of high-quality atomic charges. AM1-BCC model - II. Parameterization and validation.” *J. Comput. Chem.* **23**, 1623–1641 (2002).
- [51] T. Darden, D. York, and L. Petersen, “Particle mesh Ewald: An N log(N) method for Ewald sums in large systems,” *J. Chem. Phys.* **98**, 10089 (1993).
- [52] Ryan Gotchy Mullen, Joan-Emma Shea, and Baron Peters, “Transmission Coefficients, Committors, and Solvent Coordinates in Ion-Pair Dissociation,” *J. Chem. Theory Comput.* **10**, 659–667 (2014).
- [53] Benjamin Lickert and Gerhard Stock, “Modeling non-Markovian data using Markov state and Langevin models,” *J. Chem. Phys.* **153**, 244112 (2020).
- [54] Dedi Wang, Renjie Zhao, John D. Weeks, and Pratyush Tiwary, “Influence of long-range forces on the transition states and dynamics of NaCl ion-pair dissociation in water,” *J. Phys. Chem. B* **126**, 545–551 (2022).
- [55] Matthias Post, Steffen Wolf, and G. Stock, “Principal component analysis of nonequilibrium molecular dynamics simulations,” *J. Chem. Phys.* **150**, 204110 (2019).
- [56] I. Gazuz, A. M. Puertas, Th. Voigtmann, and M. Fuchs, “Active and Nonlinear Microrheology in Dense Colloidal

- Suspensions,” *Phys. Rev. Lett.* **102**, 248302 (2009).
- [57] J R Gomez-Solano and C Bechinger, “Probing linear and nonlinear microrheology of viscoelastic fluids,” *EPL* **108**, 54008 (2014).

Supporting Information: Molecular origin of driving-dependent friction in fluids

Matthias Post, Steffen Wolf,* and Gerhard Stock†

Biomolecular Dynamics, Institute of Physics, Albert Ludwigs University, 79104 Freiburg, Germany.

(Dated: April 8, 2022)

I. SUPPLEMENTAL METHODS

In the main text, the simple force auto-correlation model

$$\langle \delta f(t') \delta f(t'') \rangle = \frac{\gamma}{\beta \tau_C} e^{-|t'-t''|/\tau_C} \quad (\text{S1})$$

was discussed, leading with Eq. (6) and (22) to a velocity dependent averaged friction of

$$\hat{\Gamma}(v) = \gamma \left(1 - \frac{v}{v_C} + \frac{v}{v_C} e^{-\frac{v_C}{v}} \right). \quad (\text{S2})$$

If we model a system with two characteristic time-scales, we get

$$\langle \delta f(t') \delta f(t'') \rangle = A_1 e^{-\frac{|t'-t''|}{\tau_1}} + A_2 e^{-\frac{|t'-t''|}{\tau_2}} \quad (\text{S3a})$$

$$\hat{\Gamma}(v) = \gamma \left(1 - \frac{v\hat{\tau}}{x-x_0} + \frac{v\hat{\tau}_1}{x-x_0} e^{-\frac{x-x_0}{v\hat{\tau}_1}} + \frac{v\hat{\tau}_2}{x-x_0} e^{-\frac{x-x_0}{v\hat{\tau}_2}} \right) \quad (\text{S3b})$$

$$\text{with } \gamma = \beta(A_1\tau_1 + A_2\tau_2), \quad \hat{\tau} = \frac{A_1\tau_1^2 + A_2\tau_2^2}{A_1\tau_1 + A_2\tau_2},$$

$$\hat{\tau}_1 = \frac{A_1\tau_1^2}{A_1\tau_1 + A_2\tau_2} = \frac{\tau_2 - \hat{\tau}}{\tau_2 - \tau_1} \tau_1, \quad \hat{\tau}_2 = \frac{A_2\tau_2^2}{A_1\tau_1 + A_2\tau_2} = \frac{\hat{\tau} - \tau_1}{\tau_2 - \tau_1} \tau_2.$$

Lastly, auto-correlation functions of more complex fluids are known to show the behavior of a stretched-exponential, which can be explained by an interplay of a continuous distribution of timescales, $e^{-(t/\tau)^\alpha} = \int_0^\infty d\tau' c(\tau') e^{-t/\tau'}$. This ansatz leads to

$$\langle \delta f(t') \delta f(t'') \rangle = A e^{-\left(\frac{|t'-t''|}{\tau}\right)^\alpha}, \quad (\text{S4})$$

$$\hat{\Gamma}(v) = \frac{\beta A \tau}{\alpha} \left[\gamma(1/\alpha, (v_C/v)^\alpha) - \frac{v}{v_C} \gamma(2/\alpha, (v_C/v)^\alpha) \right], \quad (\text{S5})$$

where $\gamma(a, b) = \int_0^b dt t^{a-1} e^{-t}$ is the lower incomplete gamma function.

* email: steffen.wolf@physik.uni-freiburg.de

† email: stock@physik.uni-freiburg.de

II. SUPPLEMENTAL RESULTS

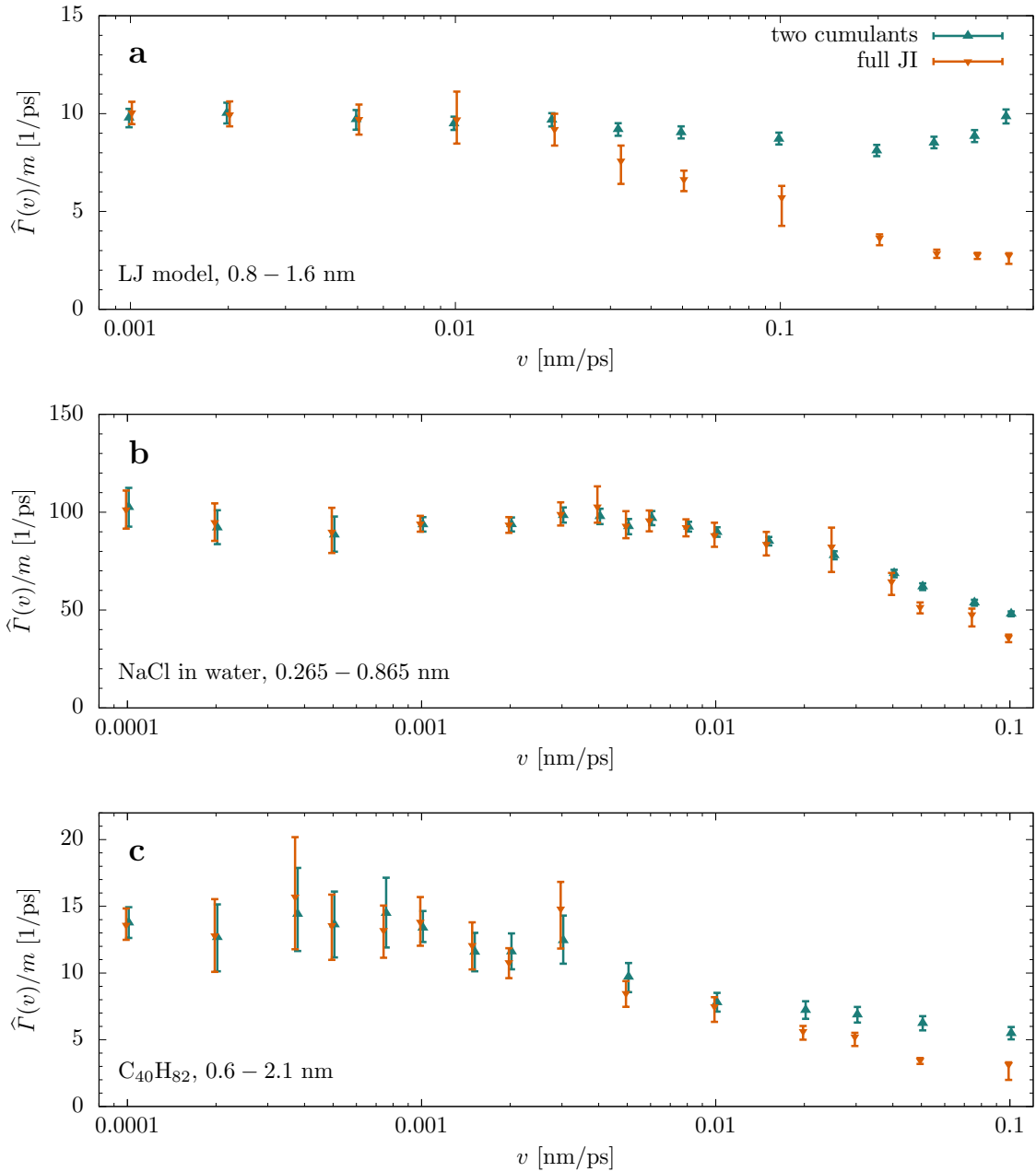


Figure S1: Comparison of the position-averaged friction [Eq. (22)] as a function of the pulling velocity v , using the cumulant approximation [Eq. (6)] and the full exponential estimator [Eq. (10)]. Shown are the results for (a) the Lennard Jones (LJ) model, (b) solvated NaCl, and (c) $C_{40}H_{82}$. While for low velocities the two estimates agree, they may differ for larger v . Here, the exponential estimate goes down faster in all cases, but most notably for the LJ model (a), despite being the simplest example of the three. The estimate of the dissipative work is higher for the cumulant approximation than using all moments, translating in higher friction than for the estimate with worse convergence behavior. The error bars indicate 95% confidence intervals estimated by bootstrapping.

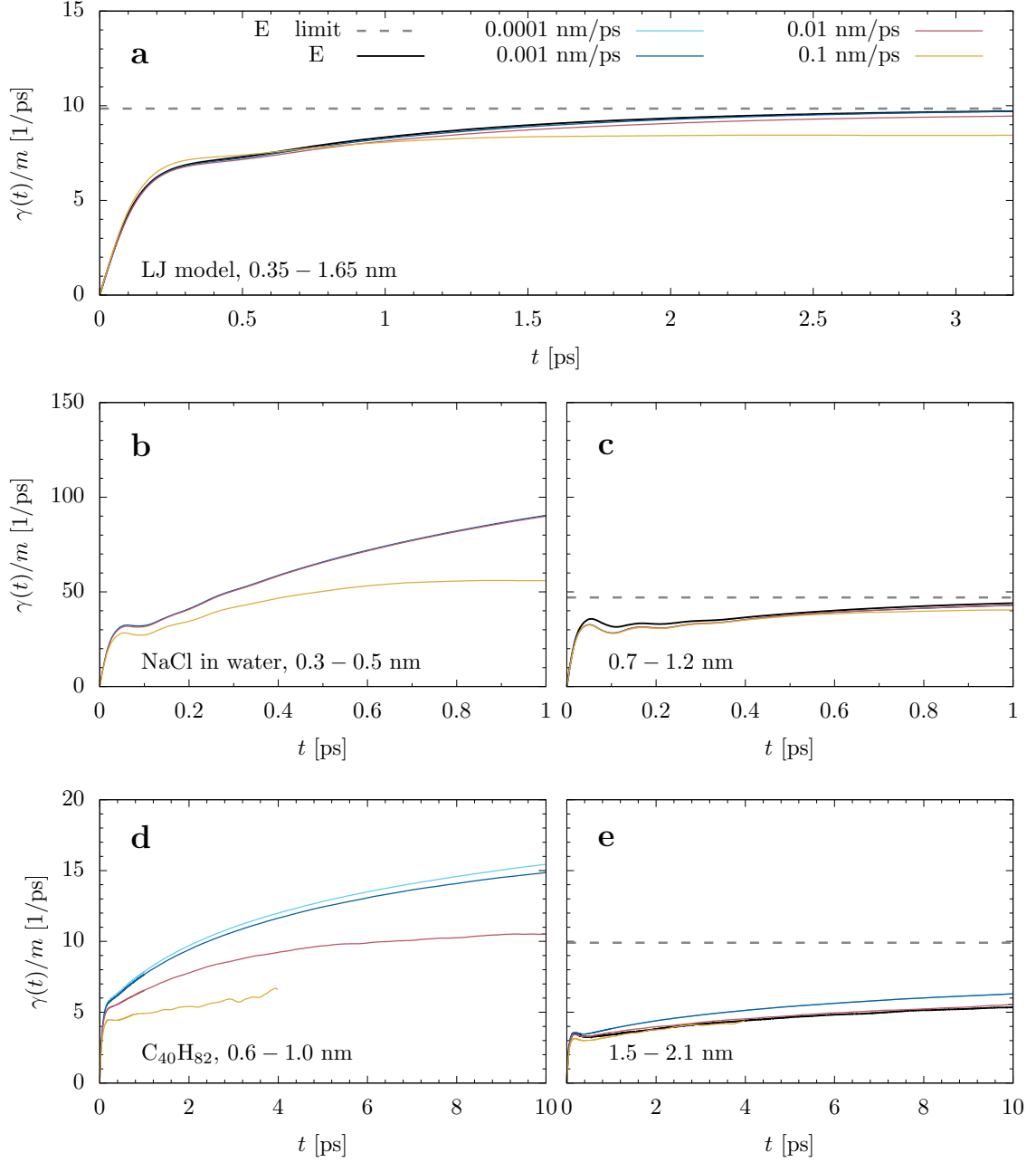


Figure S2: Convergence of friction estimate from integrating the memory kernel $\gamma(t) = \int_0^t d\tau K(\tau)$, comparing results from unbiased and pulling simulations [Eqs. (20) and (21)]. Estimates of the plateau values of the equilibrium values of the kernel are shown in dashes. In more detail, to ensure a reasonable integration, we first needed to correct, in the case of Argon and NaCl, the artificial force spike at $t=0$ due to the 10 fs time-step by employing a parabolic fit to the subsequent time frames. Moreover, since the iterative estimator Eq. (21) appeared to fail at longer times, we performed a fit of the tail to correct for the noise and to extrapolate at longer times. That is, for the Lennard-Jones model we fit a mono-exponential function to the results obtained for 0.8-1.4 ps, in order to extend the kernel from 1.4 ps onward. For NaCl we performed an exponential fit from 0.4 to 2.0 ps to connect at 0.5 ps, and for $C_{40}H_{82}$ we used a stretched-exponential fit, Eq. (S4), from 2.2 to 20 ps (resulting in $\alpha \approx 0.2$) to continue from 10 ps. These fits yield a clear plateau value, although for $C_{40}H_{82}$ this procedure might still introduce a large systematic error due to a strong dependence of the parametrization of the long-time tail. (a) For Argon, γ converges after a few picoseconds and thus, even for fast pulling velocities, the generic convergence behavior is no issue here. For NaCl, we compare $\gamma(t)$ at close (b) and far (c) ion distances. In the former case, the friction takes longer to converge to a higher value, but is still too fast to cause a generic effect. Instead, for fast v , $\gamma(t)$ converges faster and to a smaller value, explaining the decrease in Fig. (3) in the main text. In the latter case, we can compare the estimate to the kernel of the unbiased simulation, which overall tend to agree and again converge to the same friction coefficient. For $C_{40}H_{82}$ (d,e), again, for close x , the plateau value of γ is much higher than for large x , with slow, non-exponential convergence, thus potentially having a generic influence to the friction estimate of the main text. However, for fast v , there is again a faster decay to a smaller value. The generic convergence issue plays therefor again only a minor role.

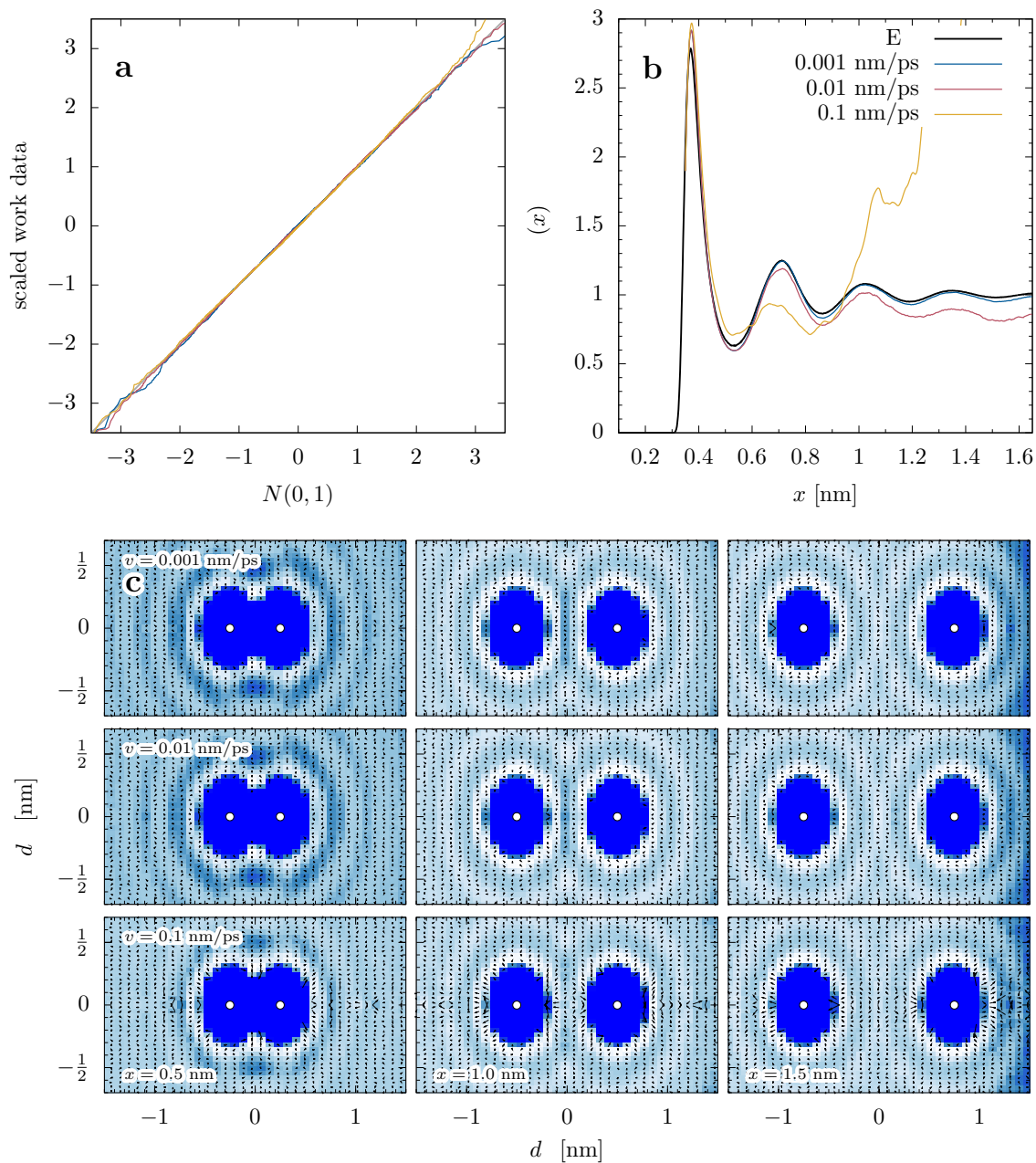


Figure S3: Supplemental information for the Lennard Jones liquid. (a) Normal probability plot of work distribution at $x = 1$ nm for different pulling velocities, showing that the distribution follows a normal shape up to noise at the very tails. (b) Radial distribution function estimated in the unbiased case by `gmx rdf` and using Jarzynski's equality for the pulling simulations via $g(x) \propto e^{-\beta\Delta G(x)}/x^2$. (c) Distribution of surrounding bath Argon atoms with respect to the distance vector of the two probe particles (white=high density, blue=small density). The arrows indicate the average parallel and perpendicular velocities of the bath particles to exclude influences of possible eddies or flows. The picture is mirrored at the horizontal axis.

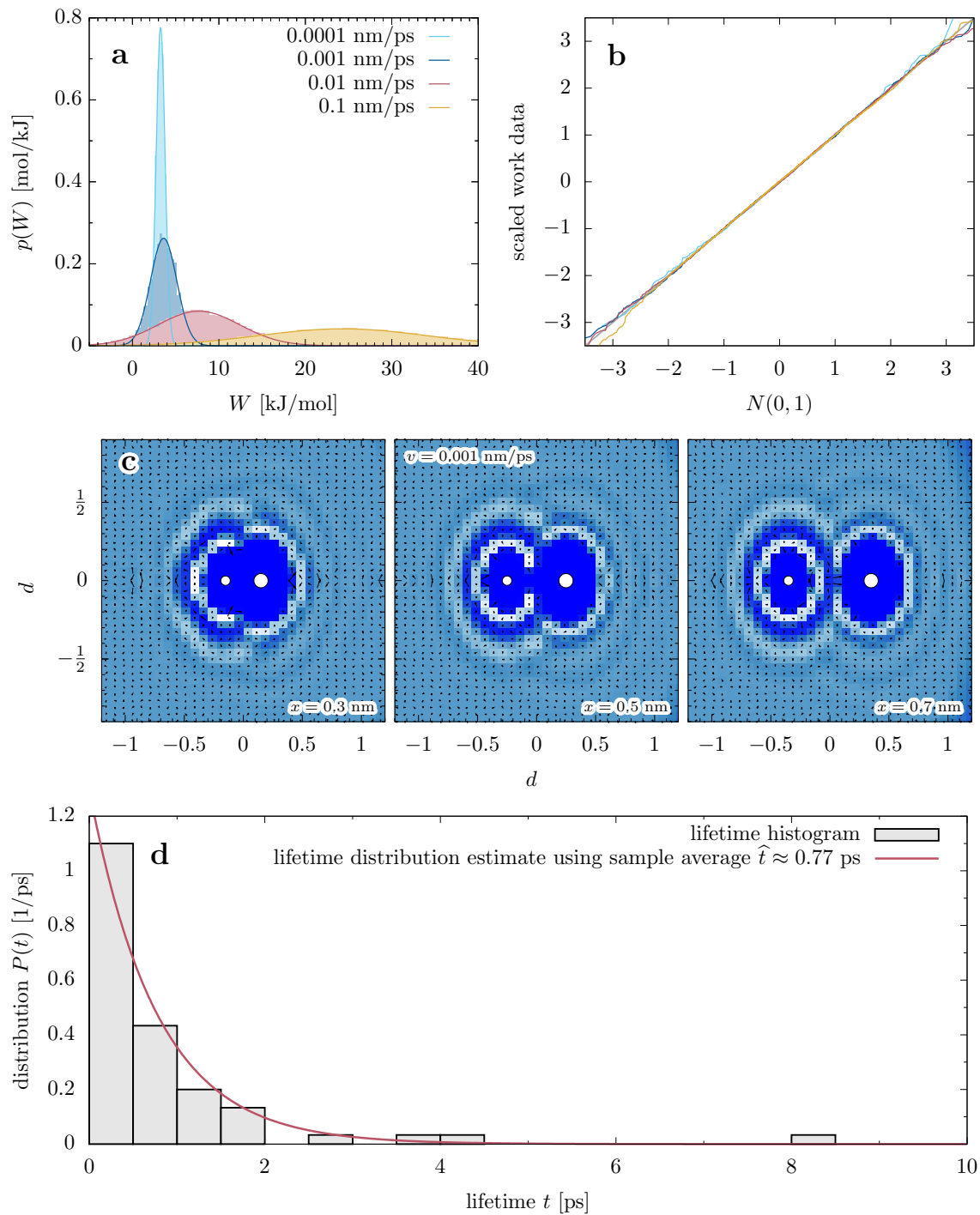


Figure S4: Supplemental information for NaCl in water. (a,b) Work distribution at 0.53 nm for different pulling velocities. While the distribution clearly gets broader, it still follows a normal shape up to noise at the very tails. (c) Distribution of surrounding water oxygen atoms with respect to the distance vector of the two ions (white = high density, blue = small density). The arrows indicate the average parallel and perpendicular velocities of the bath particles to exclude influences of possible eddies or flows. The picture is mirrored at the horizontal axis. (d) Lifetime distribution of waters inside the first shell.

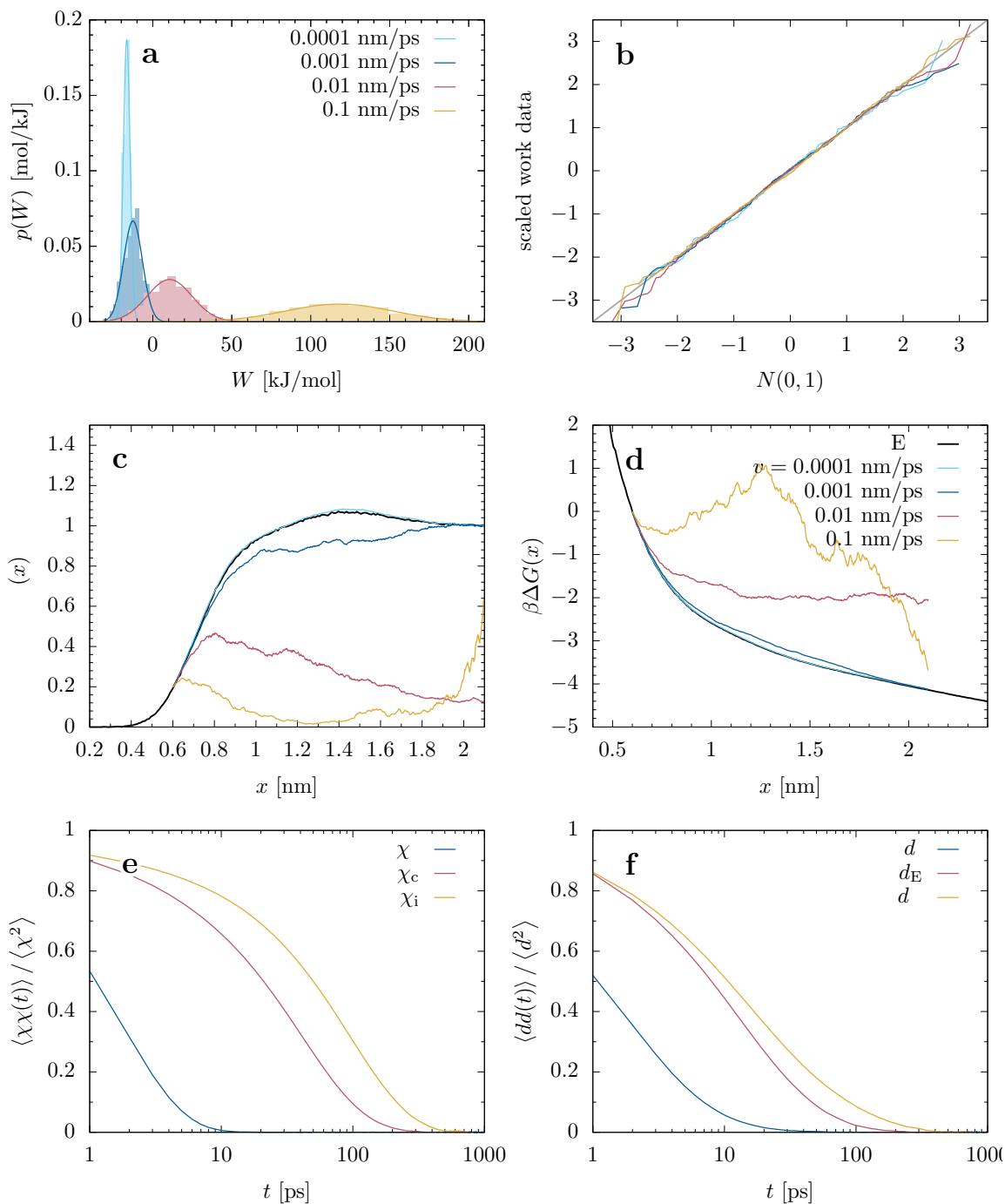


Figure S5: Supplemental information to $C_{40}H_{82}$ bulk liquid. (a,b) Work distribution at $x = 1.4$ nm for different pulling velocities. While the distribution clearly gets broader, it still follows a normal shape up to noise at the very tails. (c,d) distribution of x as radial distribution and free energy, respectively. Due to the complex shape of the alkanes, the estimate becomes poor already for moderate pulling velocities due to poor convergence of Jarzynski's equality. However, since we believe that the work variance itself is estimated properly, we may still trust the resulting friction (and the statistical error visualized by the error bars, e.g. in Fig. S5). (e,f) Auto-correlation of internal coordinates of individual alkanes parametrizing their shape. While there are no clear collective motions of the arms, we can still estimate the time-scales of individual movements, e.g., that of the dihedral angles at the center and the tips (see Fig. 4a of the main text), as well as the arm distances, which happen from a few to hundreds of picoseconds.